Autonomous Robots manuscript No.
(will be inserted by the editor)

Contact type dependency of texture classification in a whiskered mobile robot

Charles W. Fox · Ben Mitchinson · Martin J. Pearson · Anthony G. Pipe · Tony J. Prescott

Received: date / Accepted: date

Abstract Actuated artificial whiskers modeled on rat macrovibrissae can provide effective tactile sensor systems for autonomous robots. This article focuses on texture classification using artificial whiskers and addresses a limitation of previous studies, namely, their use of whisker deflection signals obtained under relatively constrained experimental conditions. Here we consider the classification of signals obtained from a whiskered robot required to explore different surface textures from a range of orientations and distances. This procedure resulted in a variety of deflection signals for any given texture. Using a standard Gaussian classifier we show, using both hand-picked features and ones derived from studies of rat vibrissal processing, that a robust rough-smooth discrimination is achievable without any knowledge of how the whisker interacts with the investigated object. On the other hand, finer discriminations appear to require knowledge of the target's relative position and/or of the manner in which the whisker contact its surface. (146 words)

Keywords whiskers · vibrissae · tactile sensing · texture discrimination

Charles W. Fox, Ben Mitchinson and Tony J. Prescott
Adaptive Behavior Research Group
Department of Psychology
University of Sheffield
Tel.: +44(0)114 222 6591
Fax: +44 (0)114 276 6515

Martin J. Pearson and Anthony G. Pipe
Bristol Robotics Laboratory
Du Pont Building
Bristol Business Park
Coldharbour Lane
Frenchay
Bristol
Tel.: +44(0)117 328 6321

1 Introduction

The long facial whiskers (macrovibrissae) of rodents such as rats and mice provide these animals with a sophisticated and multi-functional tactile sensory apparatus [21], [8]. Using their vibrissae, rats are able to make fine-grained discriminations based on surface texture with a resolution similar to that achieved by the human fingertips [10]. The exploration of texture by the vibrissae is an active process which involves sweeping ('whisking') the whiskers across the target surface at a rate of 5-15Hz during typical exploratory behaviour [4]. The brushing of each vibrissa against the target surface induces vibrations in the whisker shaft that are transduced into neural signals by mechanoreceptors in the whisker follicle [23]. The neural encodings of these vibration patterns, formed across the vibrissal array, therefore provide the basis for the texture discrimination capabilities shown by the rat [1], [16]. High-speed videographic observations suggest that contact on only a small number of macrovibrissae over 3-5 whisking cycles is sufficient for reliable texture discrimination [10].

Tactile-based texture discrimination capabilities, similar to those of rodent vibrissae, would be useful in a variety of robot applications. For example, intelligent household appliances could use whisker-based sensing to optimise cleaning strategies to suit different surface types. Similarly, autonomous vehicles such as planetary rovers could use them to assess surface properties such as friction in order to better control locomotion and exploration [33]. Whisker sensors will be especially useful for robot local navigation and object recognition in any circumstances were the capacity to use vision sensors, or active sensors such as lasers or infra-red, is compromised by poor air quality (smoke- or dust-filled), or by turbid water. Such circumstances are often encountered

during search and rescue missions, in environments that are hazardous to humans, making the capacity to employ autonomous robots alongside human search teams particularly useful.

Research into robotic whisker systems began in the mid 1980s, and has continued since as a small but flourishing sub-field of bio-inspired engineering. The investigated solutions have differed considerably in a number of important respects. First, choice of material for the vibrissal shaft has ranged from steel wires [31], [18] through actual rat vibrissae [22], to specially-moulded composites [28]. Sensor transduction has likewise used a variety of solutions. Early robotic whisker implementations used potentiometers to measure the torque of steel whiskers as they made contact with surfaces [18]; [32]. More recent work has used electret microphones [22], resistive arrays [35], strain gauges [28], [36], piezoelectric [19], and magnetic ('Hall effect') sensors [19]; [20]. A number of systems have employed actuated whiskers in order to better simulate the active sensing capacities of the rat vibrissae. Solutions to the actuation problem have included miniaturised conventional electric motors, and actuators with more muscle-like properties such as shape-memory alloys [28] or 'air-muscles' [37]. In functional terms, previous work on robotic whisker sensing has provided proof of principle that artificial vibrissal systems can compute estimates of distance and shape [37], [36], [32], [20] and can distinguish between textures with different spatial frequencies [12], [19]. In the following we briefly summarise past research specifically related to the texture discrimination problem.

Lungarella et al. [22] investigated texture discrimination by gluing either rat whiskers, or similar-sized synthetic whiskers, to the diaphragm of an electret microphone thereby transducing vibration of the whisker shaft into acoustic signals. In one set of experiments [13] actuated whiskers, attached to a stationary robot 'head', were made to brush against a rotating textured drum. Data was analyzed as time-averaged windowed-spectra and discrimination performed by clustering vectorised spectra. When the contact period between the whisker shaft and the drum surface was known the system was able to discriminate eight distinct textures using eight whiskers with exposure to ten whisk cycles per texture (80 individual contacts); with unknown contact periods this discrimination capacity fell to five textures for the same number of whisks. In a second series of experiments [12] a 3-layer sigmoidal regression neural network was used for classification having 10 input bins for each of 6 whiskers, 10 hidden nodes, and 4 output classes. Using a controlled set of seven known head positions the system achieved 70% accuracy in classifying four textures using data from six whiskers each making a single whisk (i.e. six individual contacts). No significant gain was obtained by increasing the number of hidden nodes. In a further experiment where the robot platform was made mobile (i.e. uncontrolled head positions), classification was described as "not entirely reliable" and no quantitative results were given.

Kim and Möller [19] performed similar experiments using a non-actuated, 26mm steel whisker attached to a fixed base contacting a rotating, textured drum. Direct measurements of direction and amplitude of deflection of the whisker shaft were made with magnetic and piezo sensors. Deliberately choosing textures whose spectra did not interfere with the theoretical resonant whisker frequencies, a neural network was again used to classify the low-band spectra achieving a success rate of 85% accurate classification over seven textures. These authors noted that classification was better with shorter whiskers and that the classifier fails when the whisker base was allowed to move.

Schultz et al. [33] described a robot with 190mm whiskers whose movement was detected using strain sensors, and presented spectra for five surfaces of three types, that can be distinguished by eye. No quantitative analysis of the data were provided.

The Darwin IX robot, described by Seth et al. [35], used 40mm polyamide whiskers that, unlike natural vibrissae, can directly detect the amount of bending along the whole whisker, not just at the base. Unlike the other robots above, data was analyzed in the time domain, with 20 lagged curvature inputs fed into a biologically inspired neural network classifier. The robot was given the task of distinguishing between two textures consisting of patterns of pegs embedded in walls. In a mobile robot setting, two-way classification reached 97% accuracy, though it is unclear how many whisk cycles were typically used to make each decision.

The above systems have applied both generative methods, such as solving the beam equations to analytically remove whisker resonant frequencies [19], and data-mining methods, such as neural network training algorithms [19], [12], [22] to address the texture classification problem. An alternative approach – to be taken here – is to search for useful statistics of the data or 'features' that can then be provided as inputs to standard classifiers. Such features may be identified by careful analysis of the data, by hand or using machine methods where appropriate. This type of hypothesize-and-test method of feature discovery has produced contest-winning results in other time-series classification domains such as music retrieval [11]. A particular method for feature hypothesis generation is to examine the codes and processing mechanisms used by biological classification systems. In the domain of

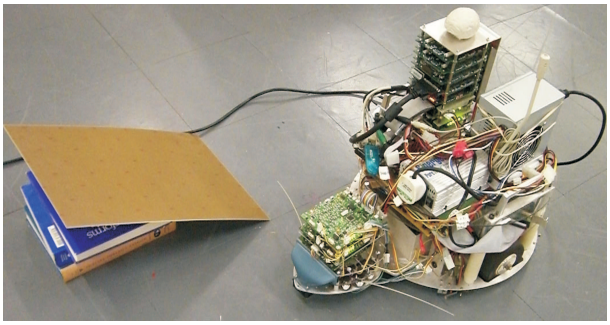

Fig. 1: WhiskerBot, whisking on a surface during the experiments.

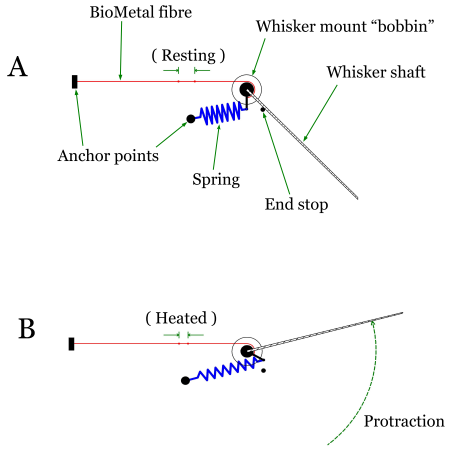

Fig. 2: WhiskerBot's actuation mechanism, in its resting (A) and heated (B) states. The BioWire contracts when heated, rotating the whisker.

vision, for instance, a classifier modeled on the primate visual cortex has recently out-performed several benchmark computer vision systems on a large database of natural images [34]. Here we will take inspiration from studies of coding in the neural pathways of the rat whisker system as one source of candidate features for resolving texture classifications problems for artificial vibrissae. One previous study [17] has taken a similar approach in which frequency-based features inspired by the analysis of activity in whisker ("barrel") sensory cortex were used to successfully classify signals obtained from an actuated 80mm metal whisker moved against textured surfaces from a known fixed starting position. The features identified by [17], along with others inspired by our own investigations of coding in the vibrissal primary afferent neurons [23], will be evaluated below for their usefulness in discriminating texture in a robotic whisker context. The performance of the above methods will also be compared with a neural network classifier.

In summary, in previous work, only [12] and [35] have attempted texture classification using artificial whisker signals obtained from unconstrained whisker-base positions and neither reported quantitative results under these circumstances. This raises the question of how robust whisker-based texture classifiers are to differences in the way in which the artificial whisker interacts with the target surface. This, in turn, is dependent on the relative position and orientation of the whisker with respect to the surface and on the nature of the whisker actuation strategy used. In the current study we therefore investigated the problem of classification of signals from different surface textures obtained using robot-mounted actuated whiskers in four different experimental settings. In the first two settings, the robot (and hence the whisker base), was stationary at one of two fixed distances from the target surface. In the third, the position of the robot with respect to the target surface was variable, as the consequence of the robot's prior movement from a fixed starting point. Finally, in the fourth setting, data was obtained from 500 arbitrary positions of the robot relative to the surface.

2 Methods

2.1 Artificial whisker system

As part of a more general investigation of functional capabilities of artificial whisker systems we previously constructed an active whisker array attached to a mobile robot platform [28,29], see figure 1. In this system each artificial whisker was a 200mm moulded glass-fibre composite rod approximately four times larger than, but respecting the general form of, a rat whisker, and gauged at the base to measure strain (bending) in two dimensions. The whisker was 200mm in length, tapered from 2mm in diameter at its base to approximately 0.7mm diameter at its tip, and the radius of curvature was 250mm.

Each whisker was actuated in a single axis (anterior-posterior) using a shape metal alloy wire (BioMetal) and a spring, shown in figure 2. Heating the BioMetal wire, using a pulse width modulated current source, caused a longitudinal contraction of the BioMetal which was translated into a rotational force around the drive shaft onto which the whisker was mounted, thereby actively protracting the whisker. When the current through the BioMetal was switched off, the wire would cool and return to its original length assisted by the spring to generate a passive retraction phase.

The drive signals to the BioMetal actuators were directly derived from a pair of coupled motor pattern gen-

erators, implemented as a spiking neural network, nominally operating as an open-loop controller. Inhibitory and excitatory projections from the strain sensors at the base of each whisker would modulate the behaviour of the pattern generators when contacts were made with the environment, thus affecting the drive signals to the BioMetal wires. This feedback control system was adopted as it best fits both anatomical (no proprioception in mystacial musculature [14]) and ethological observations (contact mediated adaptation [24]) of rats. For further details of the robot whisker morphology, actuation, and transductions mechanisms see [26], [29].

For the experiments described below a single whisker moved (whisked) at about 1Hz, and strains were sampled at 10kHz. Note that our use of strain data as input to a whisker-based texture classification system differs from previous work which has generally used direct recordings of angles and deflection amounts as classifier input.

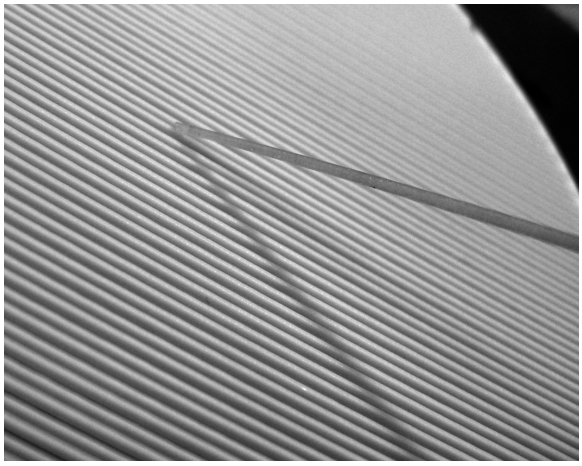

Fig. 3: Close-up of the whisker tip (and its shadow) during a typical brushing contact on the rough surface, showing the angle of contact. For brushing, the distance from robot base to surface is set to allow the whisker to sweep over the surface, making contact without sticking; for dabbing, the distance is reduced so that the whisker is pressed into a point on the surface.

2.2 Data collection

Four distinct data-sets were obtained each containing multiple trials of whisking against different textured surfaces, the difference between sets being the robot's *experimental setting*, that is, the position and movement of the robot platform relative to the investigated surface. These datasets were:

i. Fixed Brushing (FB): Here the robot platform and surface are fixed in the same positions over all trials, allowing the whisker to gently brush past the surface for about half of the whisk cycle.

ii. Fixed Dabbing (FD): Again the platform and surface are fixed in the same positions over all trials, but placed closer together than above, so the whisker covers only around 5-10mm of surface before getting stuck for the rest of the contact period. Feedback control, as described above, was switched on for fixed dabbing.

iii. Mobile Brushing (MB): The robot begins each trial away from the surface, then travels towards it before stopping and performing brushing. The initial robot positions are roughly similar across trials: starting about 1m from the surface, with a standard deviation radius of about 10mm and standard deviation orientation of about 10 degrees. The robot stops moving as soon as a surface is found, then brushing behavior is achieved by controlling whisker actuation using sensory feedback as described above.

iv. Random positions: Whisks were performed at random relative positions and orientations, as chosen by a human instructed to position the surface by hand at as wide a range of locations as possible relative to a fixed whisker base. This data thus includes both brushing and dabbing type contacts, with azimuth, elevation and radius drawn from an approximately flat distribution within the potential contact area of the whisker.

For each of (i-iii), whisks were performed against four different types of textured surface of increasing roughness: a smooth perspex sheet, fine-grade P600 sandpaper, medium-grade P240 sandpaper, and a rough perspex sheet with regular 2mm-spaced grooves. Note that sandpaper grit is non-regular, having some average number of bumps per centimeter, but not at a fixed spatial frequency. 65 whisks were obtained for each FB surface type; 52 for each FD surface type, and 34 for each MB surface type. These whisks were split into equal sized training and test sets. Contact was made by the whisker tip or within 30mm of the tip, and a typical contact is shown in fig. 3. The whisker was in contact with the surface for around 20mm of travel during brushing, and did not travel during dabbing. Heuristics were used to remove bad data which included the whisker becoming stuck on the surfaces and failing to make contact (both especially prevalent in the mobile setting). For (iv), 500 whisks each were performed against the smooth and rough perspex surfaces only.

Electronic appendix 1 shows video examples of the interaction between the whisker and smooth, P240 and rough surfaces, for settings FB, FD and MB respectively.

2.3 Feature extraction

Fig. 4 show examples of typical strain time-series data collected during the experiment in settings (i-iii). At least within each dataset, it appears possible to distinguish between data acquired from rough and smooth surfaces by eye. It is also possible to play the whisks as audio files and identify some differences by ear. Intuitively one might think of the whisker as like the needle in a record player, picking up the audio details from the record groove, however this analogy is far from perfect—in all but highly constrained situations, whiskers exhibit 'sticks, slips, skips and rings' [30] rather than smoothly brushing over the surface. For instance, both natural and artificial vibrissae often get stuck on rougher textures, then slip quickly off the sticking point and resonate (ring) at their natural harmonic frequency. Skips are like stick-slip combinations but where the whisker is not completely stopped.

We will present three pairs of simple features in addition to a replication of the neural network classifier used by [12]. The first pair of features is inspired by inspection of sampled whisker signals. The other two pairs are inspired by previous neurophysiological [2] and modeling [17], [23] investigations of the rat vibrissal system. In each case we present raw scatter plots of the data classes under the features, and confusion matrices obtained using a standard Gaussian classifier [7]. The scatter plots show all recorded data; the confusion matrices are constructed by splitting the data into equally sized (for each class) training and test sets, and reporting test performance. The Gaussian classifier operates by assuming that for each class c , data points x_i in feature space are generated by a Gaussian with unknown mean μ_c and covariance Σ_c,

$$p(x|\mu_c, \Sigma_c) = \frac{1}{Z} \exp\left(-\frac{1}{2}(x-\mu)^T \Sigma^{-1}(x-\mu)\right) \quad (1)$$

$$Z = (2\pi)^{\frac{N}{2}} |\Sigma|^{-\frac{1}{2}} \quad (2)$$

and for each class finds maximum likelihood parameters

$$\mu_c, \Sigma_c = \arg\max_{\mu_c \Sigma_c} \prod_i P(x_i|\mu_c, \Sigma_c) \quad (3)$$

for the training data in that class. On test data x_j , it assigns the maximum likelihood ('winner-take-all') class

$$c_j = \arg\max_c \prod_j p(x_j|\mu_c, \Sigma_c). \quad (4)$$

3 Results

3.1 Neural network replication

We first give results for a standard neural network classifier as used in previous studies. Following the methodology of [12], the strain time-series from a portion of the contact period was Discrete Fourier Transformed (DFT), convolved with a 70 point Blackman window, and quantized into 10 bins. Unlike Fend et al., our data does not contain information about the start and end of the contact periods, and contact periods are highly variable in the mobile setting especially. Therefore we made use of the onset detector described below to estimate the start point, and took a conservative 1024 points of time series following it for the analysis. As in Fend et al., a three-layer multilayer perceptron was used, having between 10 and 14 hidden nodes. We used neurons with the transfer function $y = 2/(1 + \exp(-2x)) - 1$ for hidden and output layers with one output node per class, and target values of ± 1. Classification was by winner-take-all and training used the Levenberg-Marquardt numerical optimisation algorithm [7]. (Window size, transfer function and output representation were not detailed by Fend et al., therefore we chose the best-performing values found by trial and error.) The training regime of Fend et al. was replicated: the network was trained ten times from random initial weights and on random test and training partitions of the data, and the best test set performance is reported.

The confusion matrices in Table 1 give results for the individual settings (*FB*=Fixed Brushing; *FD*=Fixed Dabbing; *MB*=Mobile Brushing) and for a single network trained on all three (*ALL*) settings together. The confusion matrix rows represent the true classes and the columns the predicted classes (hence perfect classification would correspond to zeros in all table elements except the diagonals) Assuming a reference Beta prior [5] on the probability of correct classification, the posterior expectation and standard deviation (a confidence measure) of this probability are presented as percentages in the accompanying text.

We note that the neural network method gives good classification performance *within* each setting – including the mobile brushing case – but does not generalize particularly well across the settings.

3.2 Onset and Offset features

On listening to whisks from the dabbing experiment by playing them as sound waves it was apparent that whisks of rough surfaces featured pronounced clicks during the onset and offset of contact.

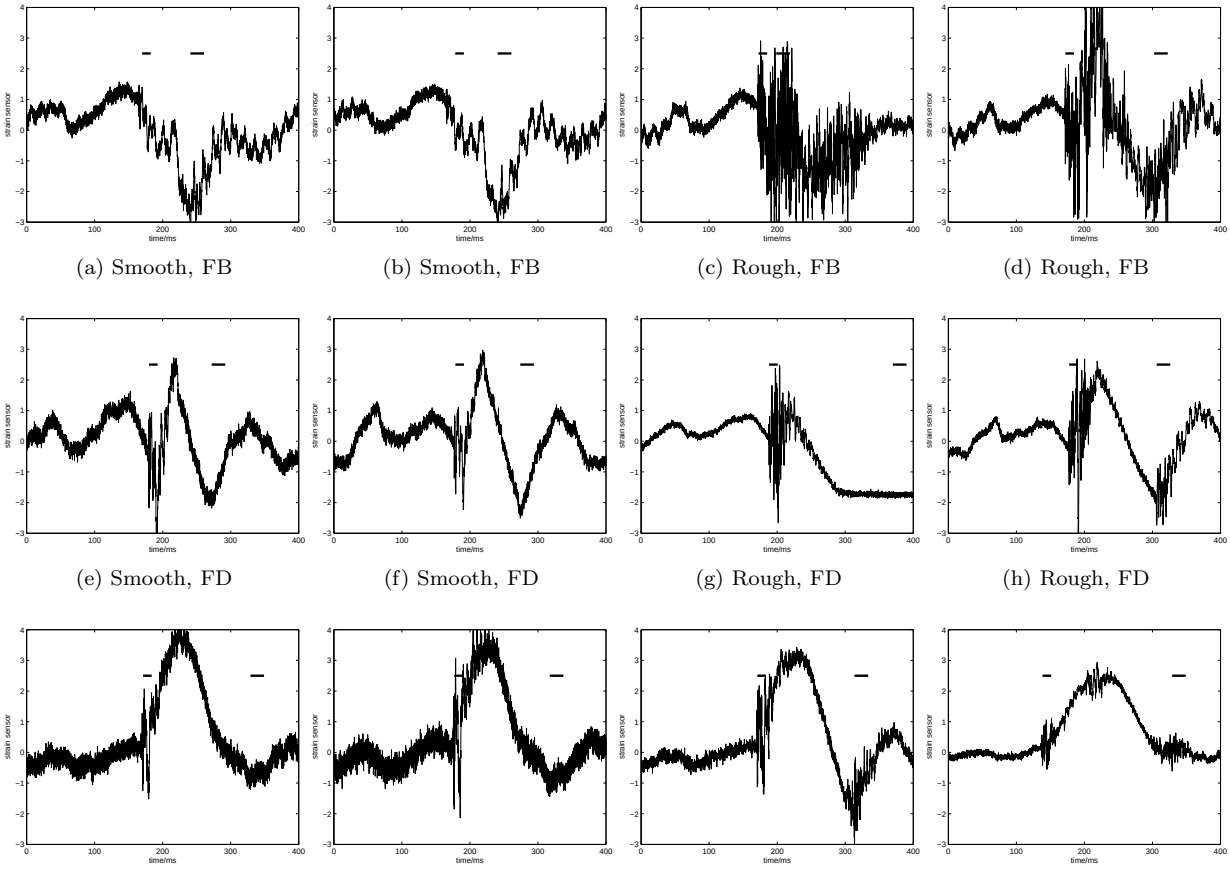

(a) Smooth, FB (b) Smooth, FB (c) Rough, FB (d) Rough, FB

(e) Smooth, FD (f) Smooth, FD (g) Rough, FD (h) Rough, FD

(i) Smooth, MB (j) Smooth, MB (k) Rough, MB (l) Rough, MB

Fig. 4: Examples of whisker base strain time series data in various settings and on various textures. Two examples are shown for each texture-setting combination to illustrate variability. The horizontal axis measures time in samples (1 sample=0.1ms) and the vertical axis measures strain sensor output. The two short horizontal lines indicate the onset and offset regions, defined in section 3.2.

Further analysis (see fig. 5) showed that the onset click corresponds well to increased energy in the 2-3kHz band, in a 128 sample (12.8ms), normalized onset period. The start of the onset may be defined heuristically as the first point at which the signal's 50-sample short-term standard deviation is more than ten standard deviations away from its long-term average since the start of the whisk. Formally, for strain signal $x[t]$, and sample variance function Var, we define the onset time t_{on} by

$$\sigma^2[t] = Var(x[t-127:t]) \tag{5}$$
$$\gamma^2[t] = Var(\sigma[0:1000]) \tag{6}$$
$$t_{on} = \min\{t.\sigma[t] > 10 * \gamma[t]\} \tag{7}$$

and the value of the *onset* feature by

$$X_t[\omega] = FFT(\frac{x[t-127:t] - \langle x[t-127:t]\rangle}{Var(x[t-127:t])}) \tag{8}$$

$$onset = \sum_{\omega=25}^{35} X_{ton}[\omega] \tag{9}$$

Given this distinctive response to rough surfaces, this feature would appear to be useful for general rough/smooth discrimination. It is conceivable that the precise power distribution within this band may lead to classifiers for different surface texture frequencies such as P240 and P600 sandpaper, however we have not found such a classifier and there is much discouraging within-class variation. On the other hand, an advantage of classifying from onset data only is that is invariant to the rest of the whisk, which may vary by setting.

Energy increase in the offset as shown in fig. 6 did not appear to be limited to a particular band, but was well captured simply by the variance of the time domain signal in the 10ms period after the offset start (t_{off}, defined as the time of maximum counter-whisk-direction strain following the onset):

$$t_{off} = \arg\min t\{x[t].t > t_{on}\} \tag{10}$$

Table 1: Confusion matrices for neural network classifier. Means and standard deviations of the posterior percentage correct classification are: $FB = 86 \pm 3\%, FD = 77 \pm 5\%, MB = 85 \pm 5\%, ALL = 65 \pm 3\%$.

FB	*smooth*	*rough*	$p600$	$p240$
smooth	23	0	1	1
rough	0	23	1	1
p600	1	0	20	4
p240	0	0	4	20
FD	*smooth*	*rough*	$p600$	$p240$
smooth	15	1	3	1
rough	1	15	4	0
p600	0	2	18	0
p240	1	3	2	14
MB	*smooth*	*rough*	$p600$	$p240$
smooth	9	1	0	0
rough	1	7	0	2
p600	0	0	10	1
p240	0	0	1	10
ALL	*smooth*	*rough*	$p600$	$p240$
smooth	49	3	1	2
rough	5	31	14	5
p600	4	7	25	20
p240	2	1	13	39

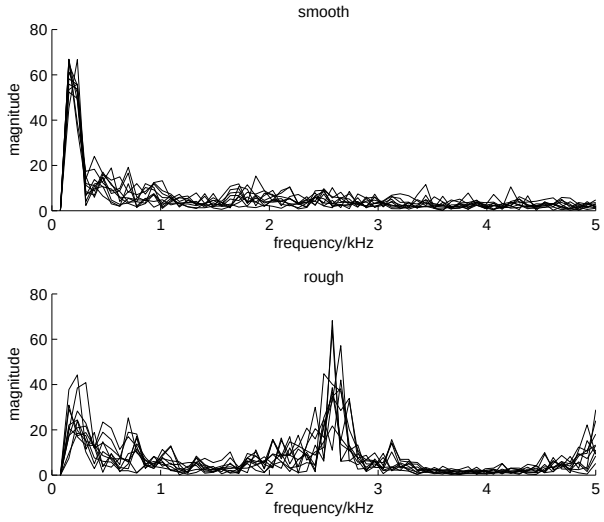

Fig. 5: FFT magnitudes for the onset region showing rough and smooth spectra for typical 128-point contact windows in the FB setting. The Nyquist frequency is 5kHz; the rough surfaces have increased power (a visible peak) around 2-3kHz which is absent from the smooth surfaces.

$$offset = Var(x[t_{off} : t_{off} + 200]) \quad (11)$$

This feature is therefore useful to discriminate between coarser surfaces such as the rough perspex and the P240 sandpaper. The offset feature may be due to the whisker sticking at the final bump of the surface – where one exists – then slipping and ringing as a result. Particularly on our rough surface, the whisker may noticeably stick in a groove and require a buildup of force to escape.

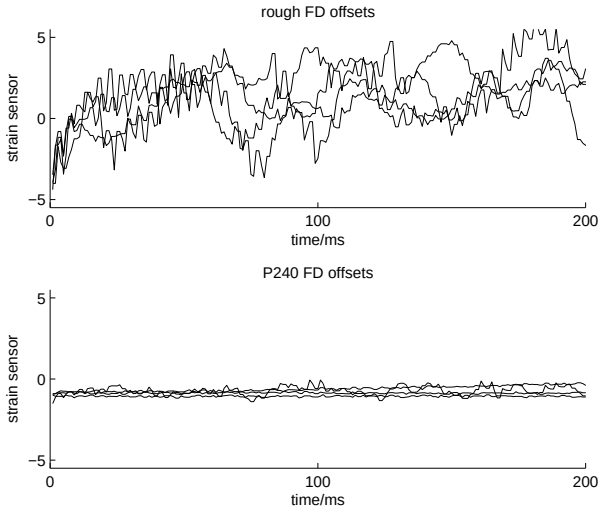

Fig. 6: Closeups of the time-domain signal at the offset ('release') stage of the whisk, for whisks against typical grooved perspex (*above*) and P240 sandpaper (*below*) in the FB setting. It can be seen that the rougher surface has much higher variance.

Table 2: Confusion matrices for the onset-offset (OO) classifier. Means and standard deviations of the posterior percentage correct classification are: $FB = 87 \pm 3\%, FD = 67 \pm 6\% MB = 52 \pm 8\%$.

FB	*smooth*	*rough*	$p600$	$p240$
smooth	28	0	1	3
rough	0	32	1	0
p600	1	0	26	5
p240	3	0	4	26
FD	*smooth*	*rough*	$p600$	$p240$
smooth	19	0	2	5
rough	1	25	0	0
p600	3	1	17	5
p240	6	1	10	9
MB	*smooth*	*rough*	$p600$	$p240$
smooth	12	0	2	2
rough	0	10	1	5
p600	1	7	7	2
p240	2	9	0	6

Fig. 7 shows that both of the above features are useful across the first three experimental settings. Specifically, the binary rough *vs.* non-rough onset regions are in similar positions across all datasets. This is important as it shows that they are not due to non-texture-related artifacts in individual settings. Conversely, the more finer-grained, offset discrimination between sandpaper and rough perspex is possible *within* each setting, but these regions vary greatly *between* settings.

We applied the same maximum-likelihood ('winner-take-all') Gaussian classifier and confusion matrix analysis as in the neural network model, to give the results of Table 2 for the individual settings.

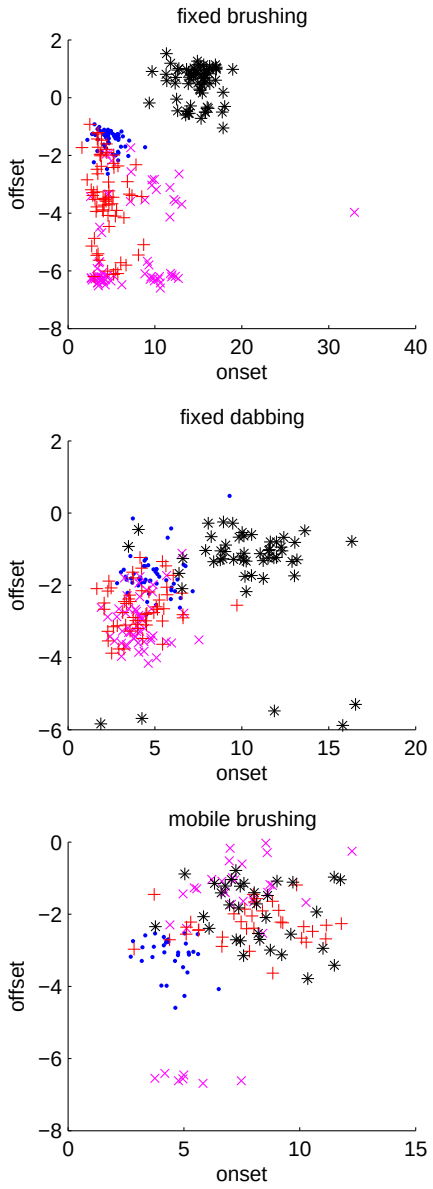

Fig. 7: Onset and offset (OO) feature values for data sets i–iii. Textures are: smooth perspex sheet (dots), fine-grade P600 sandpaper ('x's), medium-grade P240 sandpaper ('+'s), and rough perspex sheet with regular 2mm-spaced grooves ('*'s).

3.3 Biologically inspired frequency features from Cortical responses

Recordings of neuronal firing patterns obtained from cells in the whisker sensory ("barrel") cortex of anesthetized, head-fixed rats whisking against textured surfaces suggest the possibility of using frequency-based features to perform texture classification. *In vivo* animal experiments [2] played pure sinusoidal vibration stimulations into whiskers and found cortical cells responded to the product $X\omega$ of the amplitude and frequency of these vibrations. Texture experiments [3] generalized this, playing back pre-recorded texture vibrations, and the best found feature responded to by cortical neurons was

$$\langle X\omega \rangle = \int_{\Omega} \int_{T} |X(\omega, t)| \omega d\omega dt \tag{12}$$

This is equal to the amplitude-weighted mean frequency, or *centroid*, averaged over time. This same feature has been found useful in musical audio analysis [11], as it can represent the average musical pitch. Musical classifiers often use it in conjunction with a 'total energy' feature which gives information about the onset type of musical nodes, analogous to the onsets of whiskers contacting a surface: this suggests trying the energy feature in the whisker texture domain too. In our analysis, the average over time is implicit as we work with a large-window DFT containing all time points of interest.

[17] proposed that the centroid and energy of the contact period spectrum could correspond to the *physical* frequency and depths of bumps in the texture surface. Hipp et al. then tested this hypothesis in experiments in which actuated 80mm steel whiskers were moved against a variety of textured surfaces. For each whisk the spectrum of the whole whisk cycle was then analysed for the centroid and energy features which were input into a Gaussian classifier as in section 2.3. This system achieved 75% of the classification accuracy of a Gaussian classifier based on the entire binned spectrum (similar to our neural network in section 3.1), showing it to be a useful statistic of the spectrum with respect to the classification task.

Following these precedents we investigated the suitability of frequency-based classification of data from our own robotic whisking data. To obtain the required features we first low-pass filtered the lower fifth of the DFT spectrum to remove overall bending effects as in [17]. Here the DFT was taken over the whole contact period, excluding onset and offsets, which in the mobile robot setting (iii) was of variable length, therefore the centroid was normalized in the spectral domain (as the DFT is of variable size), and the energy normalized per unit time as follows:

$$centroid = \frac{1}{N} \sum_{\omega=N/5}^{N} \omega.X[\omega] \tag{13}$$

$$energy = \frac{1}{N} \sum_{\omega=N/5}^{N} X[\omega] \tag{14}$$

Table 3: Confusion matrices for centroid-energy (CE) classifier. Means and standard deviations of the posterior percentage correct classification are: $FB = 56 \pm 5\%, FD = 42 \pm 7\%, MB = 41 \pm 9\%$.

FB	*smooth*	*rough*	*p*600	*p*240
smooth	25	0	5	2
rough	0	30	0	3
p600	20	1	2	9
p240	8	8	2	15
FD	*smooth*	*rough*	*p*600	*p*240
smooth	22	0	3	1
rough	11	5	5	5
p600	3	2	9	12
p240	2	1	15	8
MB	*smooth*	*rough*	*p*600	*p*240
smooth	9	4	3	0
rough	1	7	5	3
p600	3	4	7	3
p240	4	3	6	4

Results using these frequency features are shown in Figure 8 and Table 3. For the fixed brushing experiment, the features performed excellently, separating smooth perspex, P240 sandpaper and rough perspex. However for the dabbing and mobile brushing settings their utility deteriorates greatly. In the dabbing case the difficulty is that there is only a short non-onset contact period in which to examine the spectrum before the whisker becomes stuck against the surface. The mobile case is more interesting, however, here variability in the distance and angle to the surface appears to detract from the usefulness of frequency features as the same surface at a larger distance will produce a higher frequency due to the increased whisk radius.

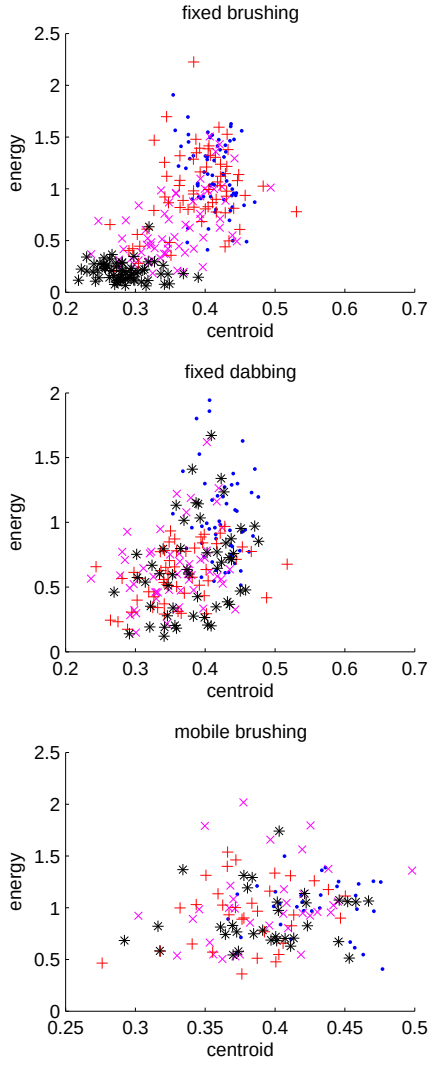

Fig. 8: Frequency centroid and energy (CE) features for experimental settings i-iii. Textures are: smooth perspex sheet (dots), fine-grade P600 sandpaper ('x's), medium-grade P240 sandpaper ('+'s), and rough perspex sheet with regular 2mm-spaced grooves ('*'s).

3.4 Biologically inspired features from the whisker primary afferents

In previous work [23], [27] we constructed a biomimetic model of transduction in the whisker follicle. This electromechanical model transforms patterns of mechanical whisker stimulation into their initial encoding as patterns of neural firing in primary afferent neurons (PAs) associated with each whisker follicle. This PA activity is passed up to the brainstem trigeminal sensory complex via the trigeminal nerve. Statistics of the spike trains from these simulated PAs may be used to drive a texture classifier.

The first part of the model is a mechanical simulation of the components of the follicle, including the whisker itself. External inputs are forces from the muscles and elastic tissues driving the follicle capsule to whisk, along with forces applied to the whisker shaft or tip by environmental obstructions. The output of the mechanical model is the strains in the tissues that are the seat of various whisker follicle mechanoreceptor families. In particular, the model derives tissue strains that are Rapidly Adapting (RA) or Slowly Adapting (SA) to tonic stimuli, leading to the most often reported dichotomy in observed PA responses. The SA and RA populations in the model each comprise 20 neurons arranged in a ring around the base of the whisker, responding to strains in different orientations.

These strains form the input to the second part of the model, consisting of a number of pre-processing operations, followed by a bank of conventional integrate-and-fire models representing the PAs themselves. The pre-processing operations are derived from observations of PA responses to time-varying stimuli. Three govern instantaneous response: gain, projection onto a vector representing maximal sensitivity (the whisker deflections are vectors), and a nonlinear response curve. In addition, temporal response is represented through stimulus adaptation and stimulus memory.

Responses of the model to simple passive whisker deflections are not complex: for example, step deflections generate phasic and tonic responses through RA and SA afferents, respectively. Responses to more complex stimuli are much less intuitive and comparable biological data are generally lacking. The results presented here use the model of [23] – the revised model of [27] would give similar values for the simple features used here.

Examples of simulated RA and SA responses obtained from the whiskered robot in the FD setting are shown in Figures 9a, 9b and 9c, along with the raw strain data for comparison. We next examine the utility of these responses as features.

On inspection, the local RA rates (summed over the 20 neurons in the population) appear to function well as an onset detector, so can be used to replace our previous, hand-picked onset detector. We use a fixed threshold to first detect the *presence* of an onset, and then employ the mean firing rate during the following 10ms period as our onset *feature* (for use in texture classification). Following the onset, SA cells continue to fire at rates which depend on both the amplitude and frequency of the whisk wave. We therefore used the mean firing rate of the SA cells (summed over the population) during a 100ms post-onset period a second feature. Fig. 10 and Table 4 show the performance of this RA/SA feature pair. As with the other features, the PA classifier separates well within each setting, but the classification boundaries are different across settings (note the changes of scale on the axes especially).

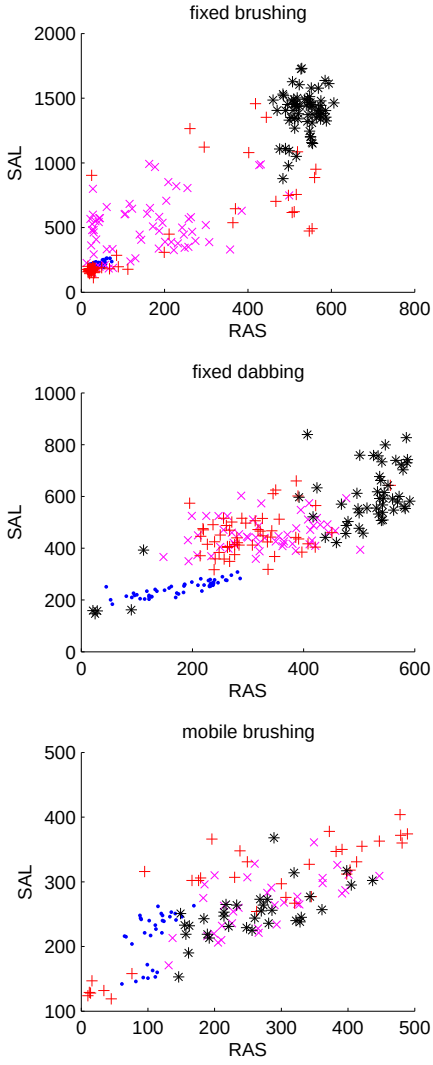

Fig. 10: Slowly Adapting (SAL) and Rapidly Adapting (RAS) simulated primary afferent (PA) cell firing rate features. Textures are: smooth perspex sheet (dots), fine-grade P600 sandpaper ('x's), medium-grade P240 sandpaper ('+'s), and rough perspex sheet with regular 2mm-spaced grooves ('*'s).

3.5 Across-setting results

While we do not have enough data from settings (i-iii) to form a sufficient sample from all possible whisker-base position and angle settings, it is still of interest to plot all three of these data sets on the same axes, in order to visualize how the features perform in a more general environment. Recall that most previous animal and robotic work has performed classification in some single 'head-fixed' setting only, raising the concern that such classifications may not generalize beyond those specific circumstances. Results from this across-setting analysis are shown in fig. 11. The subsequent three confusion matrices correspond to the three feature pairs (OO=onset-offset; CE=centroid-energy; PA=primary afferent) when used on the inter-setting data as in the scatter plots.

All the features except offset seem reasonably useful for generalized binary rough-smooth classification: however the 3 frequency-based features (including SA

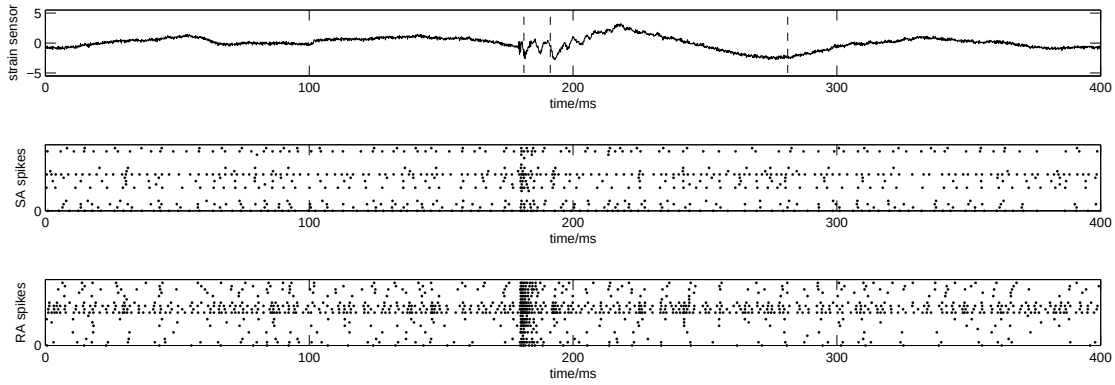

(a) Smooth perspex

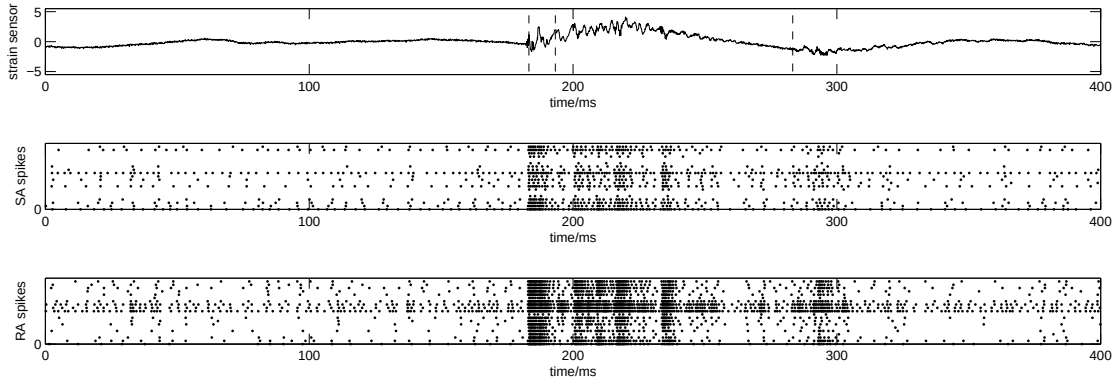

(b) P240 sandpaper

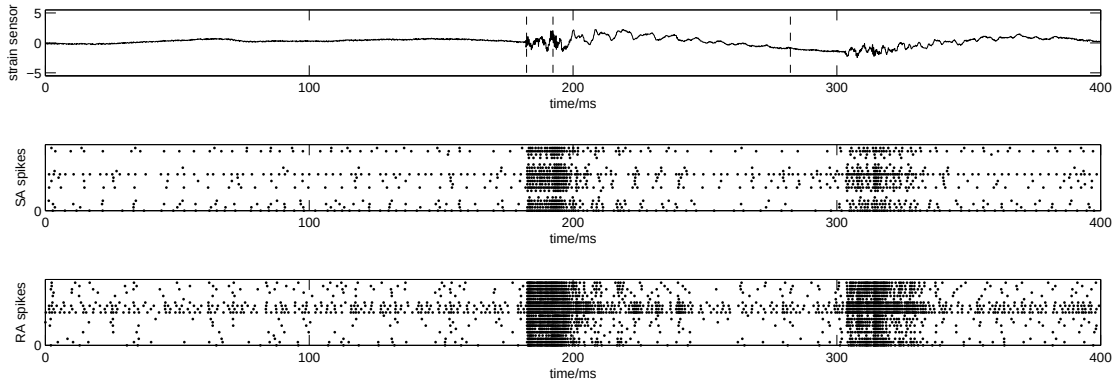

(c) Rough perspex

Fig. 9: Examples of raw base strain, Slowly Adapting spikes and Rapidly Adapting spikes for three textures, all in the Fixed Dabbing (*FD*) setting. Both neural populations are made of 20 neurons arranged in a circle around the whisker base, and which therefore respond to deflections in different orientations. The 20 neurons are shown along the vertical axes of the spike plots. The dashed lines indicate the start of the fixed-length contact window whose start location is determined using the RA onset detector. Summed RA activity for a short period following initial onset, to the second dashed line, forms the RA feature. Summed SA activity from the first to the third dashed lines forms the SA feature.

Table 4: Confusion matrices for primary afferent (PA) classifier. Means and standard deviations of the posterior percentage correct classification are: $FB = 76 \pm 4\%, FD = 73 \pm 5\%, MB = 71 \pm 7\%$.

FB	*smooth*	*rough*	*p*600	*p*240
smooth	32	0	0	0
rough	0	33	0	0
p600	19	1	7	5
p240	0	0	5	28
FD	*smooth*	*rough*	*p*600	*p*240
smooth	26	0	0	0
rough	1	21	0	4
p600	0	2	14	10
p240	0	1	10	15
MB	*smooth*	*rough*	*p*600	*p*240
smooth	15	0	1	0
rough	1	11	0	4
p600	2	1	11	3
p240	1	3	3	10

Table 5: Confusion matrices each classifier, over all settings. Means and standard deviations of the posterior percentage correct classification are: $OO = 60 \pm 4\%, CE = 46 \pm 4\%, PA = 61 \pm 4\%$.

OO	*smooth*	*rough*	*p*600	*p*240
smooth	60	2	0	12
rough	4	60	4	7
p600	18	12	25	20
p240	28	7	6	35
CE	*smooth*	*rough*	*p*600	*p*240
smooth	65	2	3	4
rough	21	44	1	0
p600	35	17	7	16
p240	22	26	8	20
PA	*smooth*	*rough*	*p*600	*p*240
smooth	67	0	4	3
rough	11	52	2	10
p600	22	9	8	36
p240	11	4	5	56

rate, which depends on frequency) suffer in setting ii and iii due to the problems of short dabbing distances and variable whisk radius discussed above.

3.6 Combining classifiers

It is often possible to construct a more powerful classifier by combining features. Table 6 shows results using a 6-dimensional Gaussian classifier, operating on all three of our feature pairs (onset, offset, centroid, energy, SAL and RAS) over all settings, as in the previous section.

It can be seen that the combined classifier gives additional power in 4-way classification over all settings, and beats the neural neural network model of section 3.1. We performed a similar analysis for the case of 2-way (rough/smooth) classification, shown in table 7. In the two-way case, we found that the combined classifier

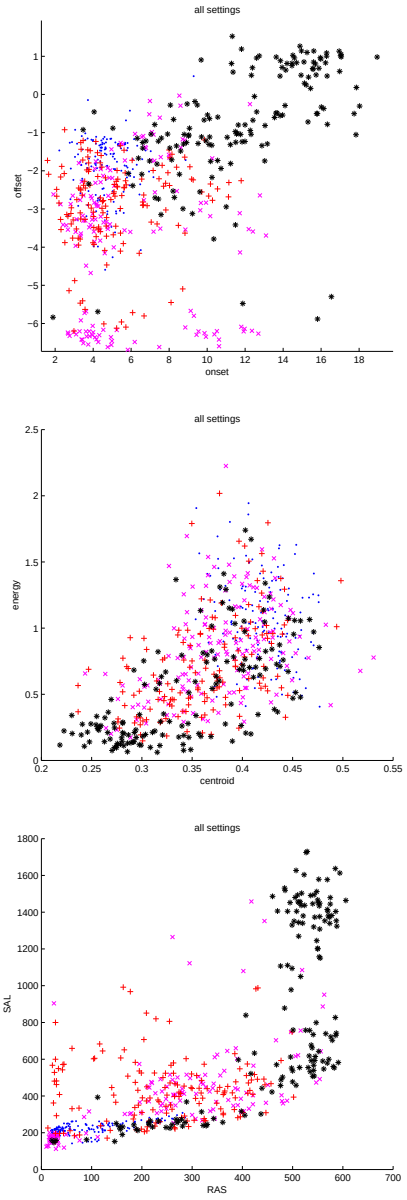

Fig. 11: Samples from datasets (i-iii) combined analysed using (a) onset-offset features (b) frequency features (c) RA/SA features as before

Table 6: Confusion matrix for the 6-dimensional, combined feature classifier, running on all settings together. The mean and standard deviation of the posterior percentage correct classification is $72 \pm 3\%$.

ALL	*smooth*	*rough*	*p*600	*p*240
smooth	67	3	3	1
rough	5	55	11	4
p600	0	32	37	6
p240	1	4	14	57

Table 7: Confusion matrices for the 6-dimensional combined feature classifier; for the three feature pairs; and for single onset and offset features; each over all settings together. Means and standard deviations of the posterior percentage correct classification are: $COMBINED = 91 \pm 2\%, OO = 92 \pm 2\%, CE = 81 \pm 4\%, PA = 91 \pm 2\%, onset = 91 \pm 2\%, offset = 78 \pm 4\%$.

COMBINED	*smooth*	*rough*
smooth	67	7
rough	6	69

OO	*smooth*	*rough*
smooth	69	5
rough	7	68

CE	*smooth*	*rough*
smooth	8	6
rough	22	53

PA	*smooth*	*rough*
smooth	74	0
rough	12	63

onset	*smooth*	*rough*
smooth	69	5
rough	8	67

offset	*smooth*	*rough*
smooth	68	6
rough	26	49

has no significant advantage over the onset-offset classifier or the PA classifier alone. Furthermore, training one-dimensional Gaussian models on the individual onset and onset features showed that the onset classifier alone achieves similar power to the combined classifier. This is of interest because the onset feature may be computed rapidly from initial contact data only, without waiting for the whisk to complete.

3.7 An online classifier

Having shown that the onset feature alone performs as well as the combination of all features in rough-smooth classification over all settings, we stress-tested this feature in the highly challenging task of classifying the 500 samples collected in setting (iv) from random whisking positions and orientations using the smooth and rough surfaces. Classification of this data was performed in real-time, requiring the use of fast cumulative update forms of the mean and (unbiased) standard deviation calculations of the T most recent strains x passed to the onset classifier:

$$\mu_t := \mu_{t-1} + \frac{1}{T}(x_t - x_{t-T-1}) \tag{15}$$

$$a_t := a_{t-1} + \frac{1}{T-1}(x_t^2 - x_{t-T-1}^2) \tag{16}$$

$$\sigma_t^2 := a_t - \frac{T}{T-1}\mu_t^2 \tag{17}$$

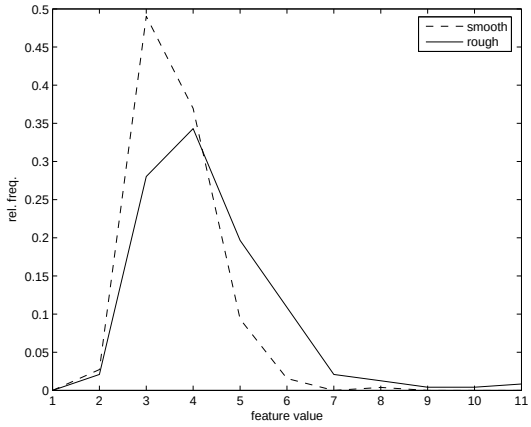

Fig. 12: Histogrammed values of a single discriminator function, from 500 whisks at random hand-held orientations and distances.

These update equations use internal state variables to avoid the need for the large sums $\mu_t := \sum_{i=t-T}^{t} x_i$ and $\sigma_t^2 := \sum_{i=t-T}^{t}(x_i - \mu)^2$ to be recomputed from scratch on the arrival of each new data point. As in the offline studies, it is necessary to obtain mean and standard deviations for every possible window location, as they are needed by the onset detector, in order to detect the *location* of the onset before classification proper begins. Fig. 12 shows the empirical distribution of the onset features in the rough and smooth classes.

The distributions are significantly different (ANOVA shows the means are different ($F(1, 495) = 53.096, p < 0.001$, partial eta squared=0.097) and Levene's test shows the variances are also different $(1, 494) = 51.466, p < 0.001$). We can compute the expected strength of belief in the correct class c after n whisks by

$$\langle p(c|d_{1:n})\rangle_{c,d} = \langle \frac{\pi(c)\prod_{i=1}^{N} p(d_i|c)}{\sum_c \pi(c)\prod_{i=1}^{N} p(d_i|c)}\rangle_{c,d} \tag{18}$$

$$= \sum_c \int_d \frac{\pi(c)^2 p(d_i|c)^{2N}}{\sum_c \pi(c) p(d_i|c)^N} \tag{19}$$

Assuming that the data were generated by the maximum likelihood parameters of two class-conditional Gaussians, and a flat prior on the classes; and computing the integral numerically with Gaussian Monte Carlo samples, we find the probability of a Gaussian classifier giving the correct class after a single whisk is 0.562, and after n whisks as shown in fig. 13. Such a classifier can be seen to achieve an expected 90% belief in the correct class after 9 whisks, 95% strength after 12 whisks, and 97.5% after 15 whisks.

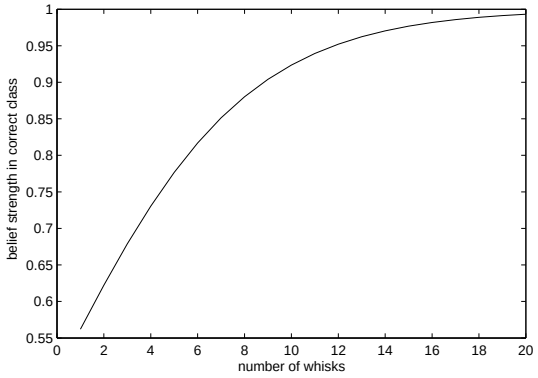

Fig. 13: Expected correct belief strength after n whisks in the random position task, using the onset feature only.

4 Discussion

This is the first work to present quantitative results in mobile whiskered texture discrimination, and the second (after [12]) to consider cross-setting discrimination. Previous studies with artificial whiskers produced good classifiers using low-level DFT features with generic parametric classifiers (e.g. 85% accuracy across 7 classes [19]) but under constrained conditions in which the interaction of the whisker with the surface was under tight experimental control. To overcome this limitation we tested several higher-level candidate features within and across three different experimental settings. Our principal findings can be summarised as follows. All candidate features tested were found to be useful within settings, i.e. where the interaction of the whisker with the surface was highly constrained. However, the frequency-based classifiers did not generalize particularly well across settings. The two best performing classifiers (see Table 7) were those based on the primary afferent model (PA) and on the onset feature. Combining all of the features produced a small accuracy improvement over the neural network replicated from [12], over all settings. The onset feature has the advantage that it can be computed very quickly following the initial contact with the surface, and gives a similar accuracy to the combined classifier in the two-class (rough,smooth) case across the settings.

The onset feature was further found to be useful for two-class (rough,smooth) discrimination across a set of highly randomized positions, requiring around 7 whisks to achieve 85% correct beliefs and 10 whisks to achieve 95% correct beliefs. In comparison, animal experiments [10] found a 85% success rate for trained rats making similar discriminations, typically making 1-5 whisks with multiple whisker contacts per whisk (46% of contacts were made with a single whisker; 36% with 2 whiskers; 18% with 3 whiskers) before the decision. For a *single* whisk (typically having two whisker contacts) the rats achieved 73% accuracy; in contrast our classifier requires three contacts to reach a similar accuracy, and reaches about 65% accuracy with only two contacts. So in this task our classifier is comparable to the rat, though the success rate is marginally lower.

We conjecture that the other features could be of more use if position and angle relative to the surface were known a priori, as we have seen that once the setting is known, good classifiers can be built using them. It is further possible that by introducing latent variables such as distance and angle from the surface, a good classifier may be found in the resulting higher-dimensioned space, generalizing over all possible settings. Frequency features in particular should be expected to be dependent on the radius and angle of contact with the surface, as physical frequencies in the texture will give rise to different whisker vibrations depending on this positioning. Methods for estimating the contact location are known (see below) and could in future be used to provide such prior information to the texture classifiers. Alternatively, the position information could be used to affect the agent's movements in order to bring the object to some standard position in the whisker field, then a simpler classifier, independent of position information, could be used. However for rapid decision-making, the onset feature provides a simple and effective way to make crude rough/smooth judgments before these more advanced inferences take place.

Which of the two above positional strategies – higher-dimensional classification and active positioning – are used by whiskered animals such as the rat? An answer to this question could inform the choice of strategy for robot platforms. There is some evidence in support of each strategy.

First, using biomechanical modeling and data obtained using plucked rat whiskers, Birdwell et al. [6] have shown that the radial distance to a point of contact can, in principle, be calculated by measuring the rate of change of moment (or equivalently curvature) at the whisker base. Further, this method has been shown to be useful for recovering distance information in an artificial vibrissal sensing system using steel-wire whiskers, gauged for strain, and fitted to a columnar whisking apparatus exploring a complex three-dimensional shape [36].

Second, behavioral data obtained by Carvell and Simons [10], in animals that were trained to discriminate texture for reward using only their macrovibrissae, provides evidence of an "active touch" strategy [25] that rats may use to optimise their texture discrimination capabilities. Specifically, they observed that while some

of the longer, more caudal, macrovibrissae were whisked back and forth across the target surface, presumably to obtain texture-related information, a number of the smaller rostralmost hairs remained in a "relatively motionless, protracted state [...] never losing contact with the surface" (p. 2641). It seems possible, then, that this use of the smaller whiskers could provide the rat with reference signals that might allow it measure, or control for, variance in the position of the larger whiskers relative to the target.

Finally, it is worth mentioning that, when allowed to do so, animals will often investigate textures with their shorter microvibrissae and other tactile sensory surfaces around the mouth [15]. In these circumstances the longer macrovibrissae may serve an important role in object detection and coarse feature discrimination, whilst also acting as a trigger for orienting movements that bring surfaces of interest into the 'foveal zone' of the shorter and more densely arranged microvibrissae (see [15] and figure 14). Contacts with this microvibrissal array, in addition to being more numerous, should be at distances and orientations that are both less variable and more predictable, thus signal features such as those considered in this article could be used – perhaps via a continuum of slow to rapid adapting afferents – to perform detailed texture classification. Brecht et al. [9] have similarly proposed that the microvibrissae may be the rats preferred tactile apparatus for making judgements regarding fine spatial detail, whilst Hartmann [15] has described rat exploration strategies in which micro- and macrovibrissal placements are either synchronized or co-ordinated in predictable sequences. Further experiments with a range of artificial whisker sensors are needed to determine whether some similar mix of short and long sensing elements, with the latter supporting a detecting/orienting capacity, might also be useful in autonomous whiskered robots.

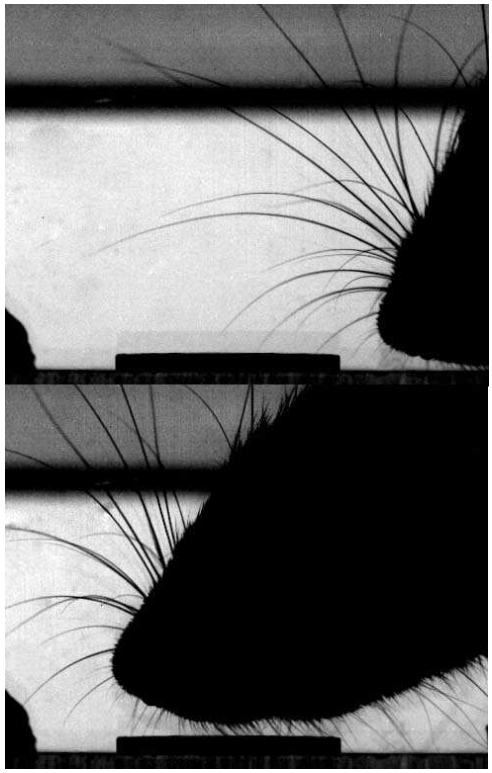

Fig. 14: Frames from a high-speed video recording (full recording in supplementary video 4) showing a rat detecting a complex textured surface of interest (a small coin) with its macrovibrissae (upper frame), and then, in a subsequent whisk cycle, investigating that surface with its microvibrissae on the chin and upper lip (lower frame). Many similar high-speed recordings obtained in our laboratory indicate that the macrovibrissae are frequently used in this manner to detect, and then orient the microvibrissal array towards, surfaces of interest.

5 Acknowledgements

The authors would like to thank members of the Active Touch Laboratory at Sheffield and the Bristol Robotics Laboratory for discussions, particularly Chris Melhuish and Robyn Grant. This work was supported by EU grants ICEA (IST-027819) and BIOTACT (ICT-215910).

References

1. M. L. Andermann and C. I. Moore. A somatotopic map of vibrissa motion direction within a barrel column. *Nat Neurosci*, 9(4):543–51, 2006.
2. E. Arabzadeh, S. Panzeri, and M. E. Diamond. Whisker vibration information carried by rat barrel cortex neurons. *J Neurosci*, 24(26):6011–20, 2004.
3. E. Arabzadeh, E. Zorzin, and M. E. Diamond. Neuronal encoding of texture in the whisker sensory pathway. *PLoS Biology*, 3(1):e17, 2005.
4. R. W. Berg and D. Kleinfeld. Rhythmic whisking by rat: retraction as well as protraction of the vibrissae is under active muscular control. *J Neurophysiol*, 89(1):104–17, 2003.
5. J. M. Bernardo and Adrian Smith. *Bayesian Theory (Wiley Series in Probability and Statistics)*. John Wiley and Sons Ltd, March 2000.
6. J.A. Birdwell, J.H. Solomon, M Thajchayapong, M.A. Taylor, M Cheely, R.B. Towal, J Conradt, and M.J. Hartmann. Biomechanical models for radial distance determination by the rat vibrissal system. *Journal of Neurophysiology*, 98(4):2439–55, October 2007.
7. C. Bishop. *Neural Networks for Pattern Recognition*. Oxford University Press, 1995.
8. M. Brecht. Barrel cortex and whisker-mediated behaviors. *Curr Opin Neurobiol*, 17(4):408–16, 2007.
9. M. Brecht, B. Preilowski, and M. M. Merzenich. Functional architecture of the mystacial vibrissae. *Behavioural Brain Research*, 84(1-2):81–97, 1997.
10. G. E. Carvell and D. J. Simons. Biometric analyses of vibrissal tactile discrimination in the rat. *Journal of Neuroscience*, 10(8):2638–2648, 1990.

11. J. Stephen Downie, Kris West, Andreas Ehmann, and Emmanuel Vincent. The 2005 music information retrieval evaluation exchange. In *Proceedings of the 6th International Symposium on Music Information Retrieval*, pages 320–323, 2005.
12. M. Fend. Whisker-based texture discrimination on a mobile robot. In *Proceedings of the 8th European Conference on Artificial Life (ECAL)*, Springer Lecture Notes in Computer Science, 2005.
13. M. Fend, S. Bovet, H. Yokoi, and R. Pfeifer. An active artificial whisker array for texture discrimination. In *IEEE/RSJ Conf on Intelligent Robots and Systems (IROS)*, Las Vegas, 2003.
14. B. T. Fundin, F. L. Rice, K. Pfaller, and J. Arvidsson. The innervation of the mystacial pad in the adult-rat studied by anterograde transport of hrp conjugates. *Experimental Brain Research*, 99(2):233–246, 1994.
15. M. J. Hartmann. Active sensing capabilities of the rat whisker system. *Autonomous Robots*, 11:249–254, 2001.
16. J. Hipp, E. Arabzadeh, E. Zorzin, J. Conradt, C. Kayser, M. E. Diamond, and P. Konig. Texture signals in whisker vibrations. *J Neurophysiol*, 95(3):1792–9, 2006.
17. J. Hipp, E. Arabzadeh, E. Zorzin, J. Conradt, C. Kayser, M.E. Diamond, and P. Konig. Texture signals in whisker vibrations. *Journal of Neurophysiology*, doi:10.1152/jn.01104.200, 2005.
18. Makoto Kaneko. Active antenna for contact sensing. *IEEE Transactions on Robotics and Automation*, 14(2):278–291, April 1998.
19. D. Kim and R. Möller. A biomimetic whisker for texture discrimination and distance estimation. In S. Schaal, editor, *From Animals to Animats 8 (Proc. 8th Intl. Conf. on the Simulation of Adaptive Behavior)*, number 8, pages 140–149. MIT Press, 2004.
20. D. Kim and R. Möller. Biomimetic whiskers for shape recognition. *Robotics and Autonomous Systems*, 55(3):229–243, 2007.
21. D. Kleinfeld, E. Ahissar, and M. E. Diamond. Active sensation: insights from the rodent vibrissa sensorimotor system. *Curr Opin Neurobiol*, 16(4):435–44, 2006.
22. M. Lungarella, V. Haffner, R. Pfeifer, and H. Yokoi. An artificial whisker sensor for robotics. In *15th Conference on Intellient Robots and Systems*, pages 2931–36, 2002.
23. B. Mitchinson, K. N. Gurney, P. Redgrave, C. Melhuish, A. G. Pipe, M. Pearson, I. Gilhespy, and T. J. Prescott. Empirically inspired simulated electro-mechanical model of the rat mystacial follicle-sinus complex. *Proc Biol Sci*, 271(1556):2509–16, 2004.
24. B. Mitchinson, C. J. Martin, R. A. Grant, and T. J. Prescott. Feedback control in active sensing: rat exploratory whisking is modulated by environmental contact. *Proc Biol Sci*, 274(1613):1035–41, 2007.
25. B. Mitchinson, C.J. Martin, R.A. Grant, and T.J. Prescott. Feedback control in active sensing: rat exploratory whisking is modulated by environmental contact. *Proc. Biol. Sci.*, 274:1035–1041, Apr 2007.
26. B. Mitchinson, M. Pearson, C. Melhuish, and T. J. Prescott. A model of sensorimotor coordination in the rat whisker system. In *From animals to animats 9: Proceedings of the Ninth International Conference on Simulation of Adaptive Behaviour, LNAI*, volume 4095. Springer Verlag, 2006.
27. Ben Mitchinson, Ehsan Arabzadeh, Mathew E. Diamond, and Tony J. Prescott. Spike-timing in primary sensory neurons: a model of somatosensory transduction in the rat. *Biological Cybernetics*, Online, January 2008.
28. Martin J. Pearson, Ian Gilhespy, Chris Melhuish, Ben Mitchinson, Mokhtar Nibouche, Anthony G. Pipe, and Tony J. Prescott. A biomimetic haptic sensor. *International Journal of Advanced Robotic Systems*, 2(4):335–343, 2005.
29. Martin J. Pearson, Anthony G. Pipe, Chris Melhuish, Ben Mitchinson, and Tony J. Prescott. Whiskerbot: A robotic active touch system modelled on the rat whisker sensory system. *Adaptive Behavior*, 15(3):223–240, 2007.
30. J. Ritt, M. Andermann, Skowronski-Lutz, E., and C. Moore. Characterization of vibrissa motion during volitional active touch. In *Barrels XIX*, Atlanta, USA, 2006.
31. R. Andrew Russell. Closing the sensor-computer-robot control loop. *Robotics Age*, 6(4):15–20, April 1984.
32. R. Andrew Russell. Using tactile whiskers to measure surface contours. In *Proceedings of the 1992 IEEE International Conference on Robotics and Automation*, pages 1295–1299, 1992.
33. A.E. Schultz, J.H. Solomon, M.A. Peshkin, and M.J. Hartmann. Multifunctional whisker arrays for distance detection, terrain mapping, and object feature extraction. In *Proceedings of the 2005 IEEE International Conference on Robotics and Automation, 2005. ICRA 2005.*, pages 2588 – 2593, 2005.
34. Thomass Serre, Aude Oliva, and Tomaso Poggio. A feedforward architecture accounts for rapid categorization. *Proceedings of the National Academy of Sciences*, 104(15):6424–6429, April 2007.
35. A. Seth, J. McKinstry, G. Edelman, and J. Krichmar. Texture discrimination by an autonomous mobile brain-based device with whiskers. In *Proceedings of the International IEEE Conference on Robotics and Automation*, volume 5, pages 4925–30, May 2004.
36. J. H. Solomon and M. J. Hartmann. Biomechanics: robotic whiskers used to sense features. *Nature*, 443(7111):525, 2006.
37. J.F. Wilson and A. Chen. A whisker probe system for shape perception of solids. *ASME Journal of Dynamic Systems, Measurement and Control*, 117:104–108, 1995.